Surface Science 606 (2012) 527–535

Contents lists available at SciVerse ScienceDirect

Surface Science

journal homepage: www.elsevier.com/locate/susc

Electroactive copper(II) bimetallic self-assembled multilayers on Si(100)

Alejandra Sánchez [a,b], Roberto Urcuyo [a,b], Diego González-Flores [a,b], Ricardo Montalberth-Smith [a], Carlos León-Rojas [a,b], Leslie W. Pineda [a,b], Mavis L. Montero [a,b,c,*]

[a] Centro de Electroquímica y Energía Química, CELEQ, Universidad de Costa Rica, San José, Costa Rica
[b] Escuela de Química, Universidad de Costa Rica, San José, Costa Rica
[c] Centro de Investigación en Ciencia e Ingeniería de Materiales, CICIMA, Universidad de Costa Rica, San José, Costa Rica

ARTICLE INFO

Article history:
Received 2 August 2011
Accepted 18 November 2011
Available online 4 December 2011

Keywords:
Copper bimetallic complex
Redox activity
Layer-by-layer
Silicon (100)
Coordination chemistry
Building block

ABSTRACT

Silicon (100) surfaces were modified by reacting 4-aminopyridine and Si–Cl bond. These surfaces were further used for tethering copper bimetallic complexes and growing monolayers and multilayers by changing the axial position via Lewis acid–base reactions. In this way, coordination chemistry approach can be used as building blocks for controlling the design of functional surfaces. Furthermore, the outcomes of the several characterization techniques indicate that the complex is spatially oriented suggesting that this simple strategy allows the preparation of three dimensional molecular structures exhibiting spatial order. The structures on surface show interesting electroactive behaviors leading two cathodic signals, that can be related to Cu(II)/Cu(I) and Cu(I)/Cu(0) electro-reduction species (signals at −0.15 V and −0.50 V) and one peak in the anodic region (−0.15 V) ascribed to the Cu(0)/Cu(II) electro-oxidation reaction, using an Ag/AgCl saturated electrode and platinum wire as reference and counter electrodes, respectively.

1. Introduction

The employment of metallic complexes functioning as building blocks via metallic atoms or ions is currently an area of great interest, because such structural arrays promote the assembly and dictate the structural features of the supramolecular products. Considerable success has already been achieved by using bimetallic bonding and polymetallic chain-like entities. These units are assembled together through axial or equatorial linker molecules, for example, amines or dicarboxylic acids, and show some properties of the multinuclear coordination compounds including their redox activity and switched electronic communication from one metal center to the other by metal-metal bond formation. Hence, the results obtained of compounds containing such metallic entities in the solid state could open a path for the construction of new molecular devices including molecular wires and interesting novel materials incorporating multimetal units. [1–10]

The enquiry of how to translate this chemistry to the silicon surface is the motivation of this research and shows the employment of copper(II) acetate as versatile and stable model of bimetallic coordination motifs. We surmise that these compounds are useful structural units for covalently-attached monolayers and self-assembled multilayers (SAMs) on Si(100) surfaces supported by the utilization of bipyridine as linker molecules between copper centers that could generate multilayers of different thicknesses, as shown in Scheme 1.

The nature of the anchoring atom and the bond formed between the molecule and the surface is important in the attachment of copper bimetallic complexes to silicon and is also one of the main challenges in the implementation of molecular/silicon architectures. In the case of Si–C, Si–O and Si–N linkages that exhibit strong bonding situation require grafting reaction conditions being relatively more aggressive compared to the functionalization when considering the self-assembly of thiol molecules on gold. In our case, the pathway studied was the reaction of 4-aminopyridine with Si–Cl-terminated surfaces leading to the formation of Si–N bond. It is generally accepted that the ability of silicon atom to act as an electron acceptor in the interaction of molecules based on Group V elements (for instance, ammonia) and is further important in controlling the overall reaction chemistry and the electron transfer. [11-15]

The integration of such cluster units onto silicon surfaces is a necessary step toward the development of novel electrically addressable and switchable functional devices. This kind of hybrid semiconductor-molecule structures have already been used to prove the conservation of the physicochemical activity of some molecular species once covalently immobilized on semiconducting surfaces. Therefore, this hybrid approach is promising for combining the advantages of semiconductor technology (doping, processing) and the large flexibility in molecular structure designing. [16–35]

In addition, since metallic copper exhibits versatile conducting material properties, the quest for aluminum replacement by copper is of

* Corresponding author at: Centro de Electroquímica y Energía Química, CELEQ, Universidad de Costa Rica, 11501 2060 San José, Costa Rica. Tel.: +506 2511 3217; fax: +506 2511 3211.
E-mail address: mavis.montero@ucr.ac.cr (M.L. Montero).

0039-6028/$ – see front matter © 2011 Elsevier B.V. All rights reserved.
doi:10.1016/j.susc.2011.11.023

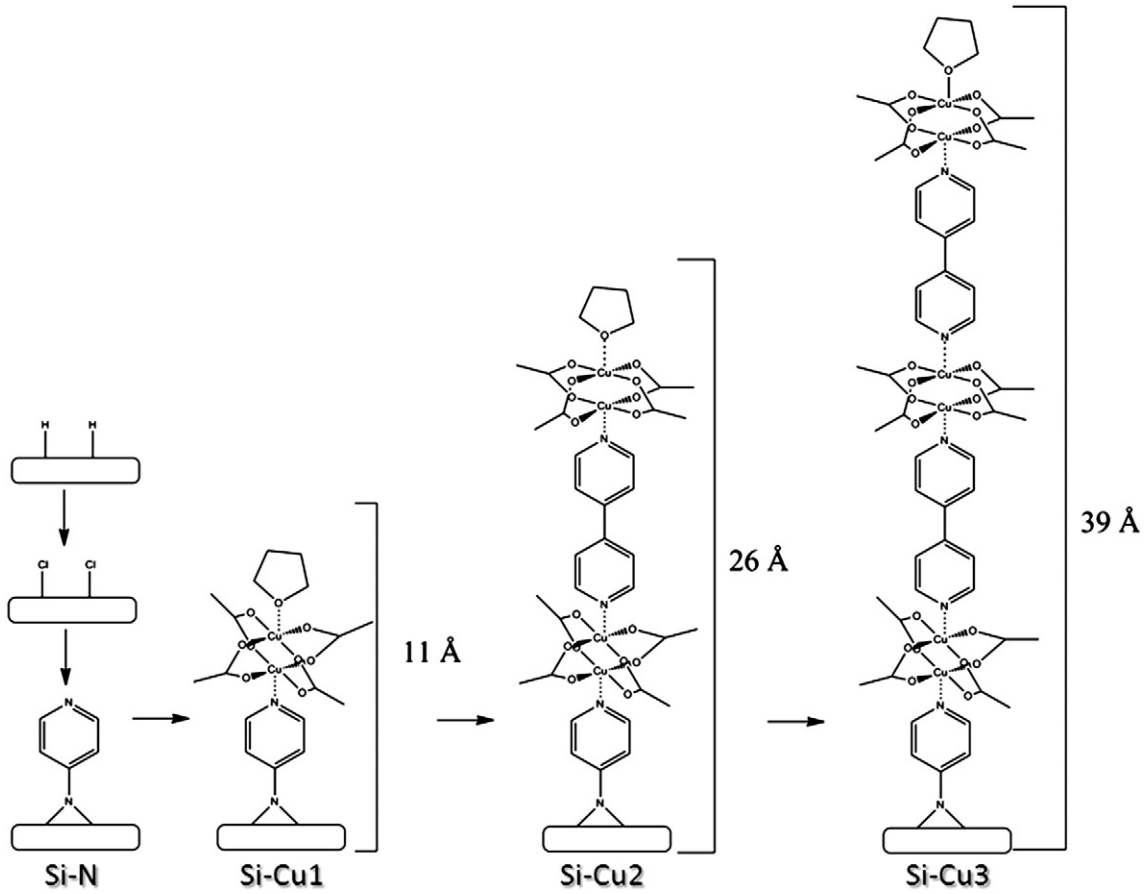

Scheme 1. Representation depicting Si(100) modification surface with copper(II) acetate growing by layer-by-layer construction. The calculated height as obtained from MM2 force field calculations using ChemDraw3D version 12.

outstanding importance for the manufacturing of microelectronic devices due to the better conductivity and superior resistance to electromigration and stress migration [36-38]. Also, the recent stringent decreasing dimensions in electronic devices, demands alternative copper sources as feedstock for fabrication at this scale. In this frame, we report on the copper(II) bimetallic self-assembled multilayers on Si(100), their characterization by X-ray photoelectron spectroscopy (XPS), contact angle measurements (CA), atomic force microscopy (AFM), X-ray reflectivity (XRR) and the electroactive behavior studies through cyclic voltammetry (CV).

2. Materials and methods

2.1. General information

All the solvents (Sigma–Aldrich) were purified and dried according to conventional procedures and freshly distilled prior to use. The compounds 4-aminopyridine (Aldrich), 4,4 -bipyridine (Sigma–Aldrich) and copper(II) acetate (Merk Co.) were used as received. The substrates were *n*-type flat silicon (100) from Ultrasil Corporation (0.001–0.002 Ω/cm).

2.2. H-terminated Si(100) surface preparation. (Si–H)

A piece of silicon (100) wafer (1 cm^2) was oxidized at high frequency for 5 min in a Harrick plasma cleaner PDC-32G, and etched with an HF solution (1%) for 3 min.

2.3. Cl-terminated Si(100) surface preparation (Si–Cl)

Si–H wafer was chlorinated in a home-made chlorine gas chamber at 80 °C for 30 min [39]. The microreactor system includes a test tube for each sample. The excess of chlorine gas was eliminated with a N_2 gas flux for 30 min.

2.4. Monolayer preparation of 4-aminopyridine (Si–N)

In the same microreactor system a piece **Si–Cl** wafer was immersed in a 4-aminopyridine solution (1 mM in THF) under nitrogen atmosphere. The reaction mixture was heated for 2 h at 60 °C, and then the functionalized wafer was washed several times with THF in an ultrasonic bath for 10 min.

2.5. Self-assembly monolayer of Si(100)-4-aminopyridine-copper(II) acetate

The wafer with **Si–N** was immersed in a copper(II) acetate solution (1 mM in THF) for 50 h. Then, the sample was washed twice in an ultrasonic bath for 10 min (**Si-Cu1**).

For multilayer formation, the **Si-Cu1** grafted sample was dipped in a solution of 4,4 -bipyridine (1 mM, THF) for 50 h at room temperature, and again 50 h in the copper(II) acetate solution (1 mM in THF) to obtain sample **Si-Cu2**. This process was repeated in order to prepare sample **Si-Cu3**. Between every new layer formation, samples were washed two times with dry THF in ultrasonic bath for 10 min.

2.6. Surface characterization

XPS measurements were performed in a Thermo K-Alpha with monochromated X-rays (12 kV, 6 mA) with a spot size of 400 μm and a takeoff angle of 90° relative to the surface, with a typical exposure time per spot (usually three spots) of 2–7 min in total to minimize beam damage. The binding energies were calibrated based on Au $4f_{7/2}$ at 83.96 eV, Ag $3d_{5/2}$ at 368.21 eV and CuLVV at 568.09 eV. Surveys were done with high pass energy (200 eV) while high resolution spectra were acquired with 50 eV of pass energy. Typical pressures during analysis were below 10^{-8} Torr.

Contact angles were determinate using a Ramé-Hart contact angle goniometer and the DropImage 2.4.05 software for data analysis. Static contact angles were determined by triplicate in several samples by depositing a sessile drop on the surface.

AFM was operating in the tapping mode (Veeco, Nanoscope IIId Digital Instruments, Santa Barbara, CA), the images were analyzed using NanoScope software. Root mean square (rms) for each substrate was calculated at least in three samples and in three different areas. Histograms were performed with WSxM 5.0 software.

Layer thickness of the modified silicon samples were characterized by Specular X-ray reflectivity (XRR). Measurements were performed using a Bruker D8 ADVANCE diffractometer, with a copper sealed tube, using a Göbel mirror as monochromation system and a scintillation counter detector. The measurements were performed using Bragg–Brentano geometry with 0.2 mm slits in the primary optics and receiving slits. Soller slits (2.5) are used to minimize angular divergence. The measurements were carried out using a step width of 0.02° and integration time per step equivalent of 7 seconds. The wavevector used are where λ is the incident angle and λ the Cu-wavelength in nanometers. Background was subtracted by performing non-specular scans for each sample with the same parameters for the specular scans. The offset angle was approximately 0.16° which was determined by the FWHM/2 of several transverse scans (rocking curves).

Cyclic voltammetry was performed with an Autolab 8-series potentiostat. The silicon substrates were mounted in a tailor-made three-electrode glass cell using an Ag/AgCl saturated electrode and platinum wire as reference and counter electrodes, respectively. Aqueous 0.1 M borate buffer was prepared by dissolving sodium borate ($Na_2B_4O_7$ $10H_2O$) in distilled water and adding 0.1 N NaOH solution to adjust the pH, then the solutions were degassed with nitrogen prior to the experiments and used as electrolyte.

3. Results and discussion

In the presence of **Si–N** functionalized surface, one can hypothesize that copper complexes self-assembled by ligand exchange with the anchored amine, in addition with THF molecules in the axial position that displaces the coordinated water molecules from the copper(II) acetate compound (**Si-Cu1**). In the same manner, Lewis acid–base interaction occurs in the presence of **Si-Cu1** and 4,4 - bipyridine linker molecules, which after addition of more copper complex leads to the self-assembled multilayer shown in **Si-Cu2**. This layer-by-layer (LbL) approach was subsequently used for the formation of the **Si-Cu3** multilayers, again by the addition of the copper(II) acetate complex and linker molecules (Scheme 1).

3.1. XPS characterization

The reaction of a primary amine with a Si–Cl-terminated surface generates a strong Si–N covalent link to the surface; however, the chemistry associated with surface preparation requires several steps, each of which could cause problems related to coverage and purity of the surface. Unfortunately the experimental conditions do not permit to test the Si–Cl sample, since it is easily hydrolyzed.

Hence, insofar as possible the Si–N samples were tested, XPS shows one peak in the N1s region at 399 eV and one peak at 285 eV in the C1s (S1, Supplementary Data), that can be assigned to amine molecules anchored to the silicon surface. [11,39] The C1s signal shows two components, C–C at 284.5 eV and C–N at 286.8 eV. The Si 2s binding energy corresponds to Si(IV) at 153.7 eV and elemental silicon at 150.0 eV, with an area relationship of 2.2: 1.0 of elemental silicon to Si(IV). [40]

In the **Si-Cu1** XPS spectra, the copper spectral region (Fig. 1A) shows split Cu peaks at 933.5 eV (2p3/2) and 953.2 eV (2p1/2) with the high binding energy satellites characteristic of copper(II). [41]

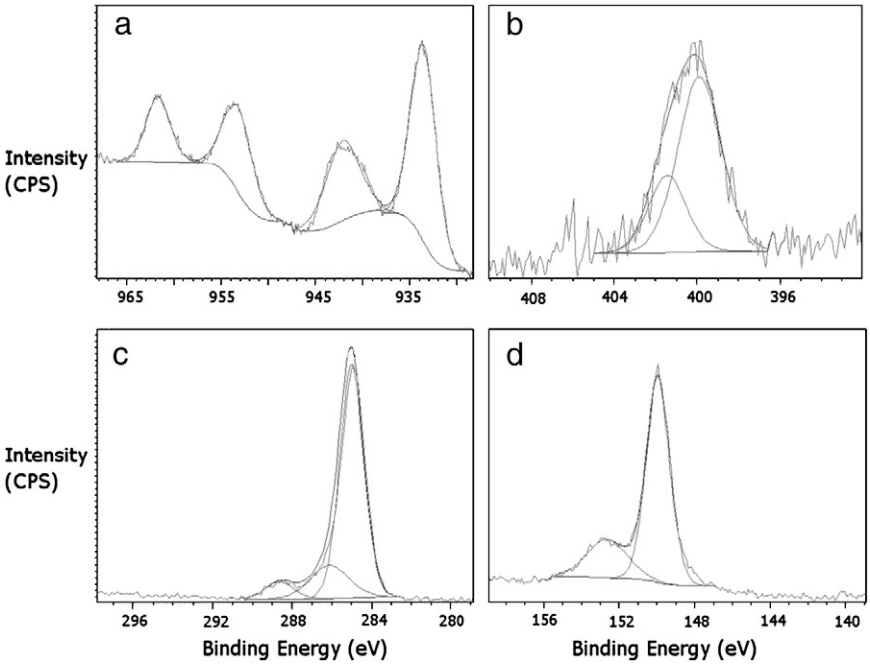

Fig. 1. The XPS spectra for **Si-Cu1**: a) copper spectral region, b) N1s, c) C1s and d) Si2s.

The carbon spectral region (Fig. 1 B) exhibits three components by deconvolution of C1s peak, with binding energies of 285.0, 286.5, and 288.6 eV, which are assigned to aliphatic carbon, C–N or CO and O–C = O bonds, respectively. [42]

In the case of the N1s region (Fig. 1C), the peak can be deconvoluted into components at 399.8 eV and 401.0 eV, consistent with amine anchored to the silicon surface and the endocyclic nitrogen from the terminal group. [39] The N1s/Cu2p ratio is 0.9:1.0; suggesting that each copper(II) acetate molecule is anchored thorough a 4-aminopyridine molecule.

The O 1s region has a peak that can be deconvoluted into two components at 530.6 eV and 532.1 eV corresponding to C–O and Si–O, respectively. [42] In the Si 2s region the peak can be resolved into two components with binding energies of 150.1 eV and 153.6 eV, with an area relationship of 2.8:1.0 corresponding to elemental silicon and bonded silicon. Based on the lattice constant of Si (100): a = 5.42 Å, and the calculated diameter of cooper(II) acetate molecule (8.72 Å), projected over the Si(100) surface, it was estimated a monolayer coverage of 1 Cu atom per 4 or 5 Si surface atom (Scheme 2). The relationship between Cu and Si(IV) derived from the XPS analysis is 1.9:12.9, a ratio that is similar to the expected value for **Si-Cu1**. Thus, this suggests that copper(II) acetate grafting strategy produces nearly a complete monolayer.

3.2. Water contact angle

The comparison of water CA of **Si–N** samples (58°) with H-terminated Si(100) surface (70°), indicates the surface modification occurred and generates a surface of hydrophilic nature. The formation of copper(II) acetate self-assembled monolayers in THF for a period of 50 h could account for the observed trend of hydrophobic surface characteristics (Fig. 2). Interestingly, the **Si-Cu1** hydrophobicity behavior is comparable with water CA reported for silicon surface functionalized with phenylethyltrichlorosilane molecules (94.7°). [43] One can speculate that THF terminal molecules (Scheme 1) and the methyl acetate group produce the hydrophobicity behavior.

The multilayers formation can be traced through the observed decrease and increase of water contact angles. When 4,4′-bipyridine is used as linker molecule it displaces the THF axial molecules on the copper(II) acetate SAMs and as a result the water CA lowers to 68° (Si-Cu1-N and Si-Cu2-N). Such transformation generates a more hydrophilic surface as expected. It is worth mentioning that water CA of modified surfaces that contain either 4-aminopyridine or 4,4′-bipyridine compare well with that of aminopropyltriethoxylsilane (APTES) modified silicon wafer surfaces. [44]

In accordance with LbL approach the assembly of copper(II) acetate layers (THF-terminated array) increases the water CA (between 90° and 98°) and the amine linker layer decreases the water CA (between 60° and 68°). Fig. 2 shows clearly such behavior, showing a route with simple coordination chemistry principles to generate new silicon multinuclear surface.

3.3. Atomic force microscopy

We studied the morphological changes following the LbL growing through tapping-mode atomic force microscopy (Fig. 3). The root mean square roughnesses (rms) for the Si samples are 1.1 ± 0.3 for Si–N, 1.0 ± 0.5 for Si-Cu1, 2.0 ± 0.2 for Si-Cu2, and 3.2 ± 0.1 for Si-Cu3. The rms values for Si–N and Si-Cu1 are very similar indicating homogenous coverage for these samples, and are also in good agreement with XPS data. In contrast, for the Si-Cu2 and Si-Cu3 samples the rms data duplicate and triplicate when compared to Si-Cu1 rms value, these findings thus suggest incomplete coverage for the second and third layers growing. The insets in Fig. 3 show the distribution of heights for each sample. This distribution is calculated by dividing the z axis in segments and measuring the population of height for each interval. The distribution of heights is directly correlated to an increase in the rms values, and at the same time, is an indirect indicator of the molecular growth over the surface. The increase in the height when going from Si-Cu1 to **Si-Cu2** samples, and from **Si-Cu2** to **Si-Cu3** samples is approximately 1.5 ± 0.5 nm, which correlates with the molecule height in Scheme 1. In this context, the complex is spatially oriented suggesting that this simple strategy allows the preparation of three dimensional molecular structures with spatial order.

3.4. XRR analysis

To further investigate the layer thickness, XRR measurements were performed. XRR experiments correlate length scales and molecular packing density over the specular wave vector Q_Z (surface normal vector), with elevated precision and reliability. The thickness of a thin layer is determined from angular positions of the subsidiary maxima or minima of a reflection curve. Fig. 4 shows X-ray intensity

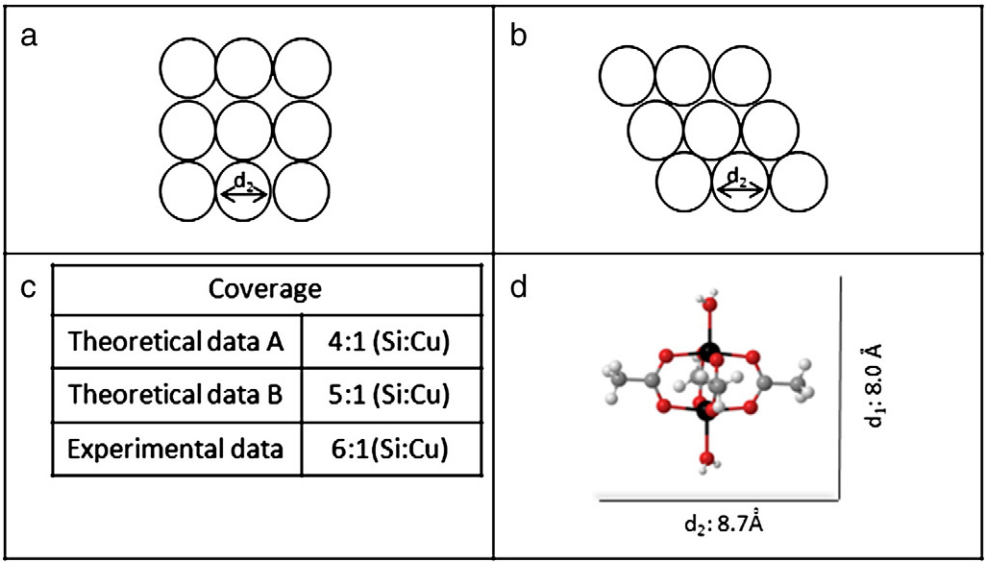

Scheme 2. Closed-packing array of copper(II) acetate molecule on Si(100) surface.

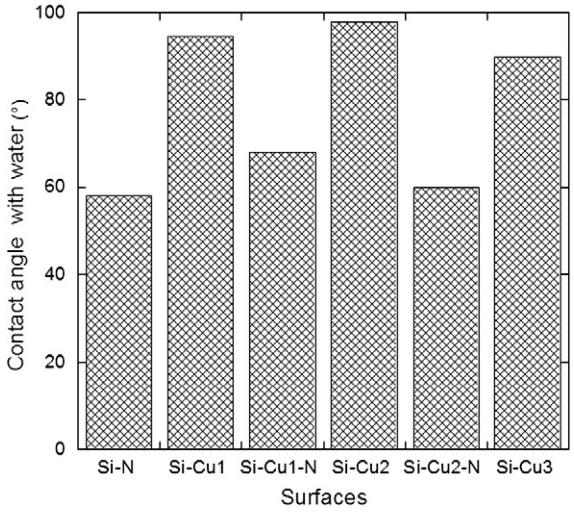

Fig. 2. Histograms of water contact angles of copper(II) acetate modified surface, and 4,4′-bipyridine terminal layer surfaces (Si-Cu1-N and Si-Cu2-N).

as a function of Q_Z of the patterns performed. In each case the background was subtracted in order to visualize better the decay.

The XRR curve in Fig. 4a.1 corresponds to **Si–H** sample acting as reference for copper grafting. [45-47] The XRR curves for **Si-Cu1**, **Si-Cu2** and **Si-Cu3** samples reveal a structural patterns that are different from **Si–H** curve (Fig. 4a.2 to 4a.4). However, the XRR curve reflections the interference patterns are not clearly observed. The weakness in the interference signals could be associated either with SAMs low packing density or to the lack of in-plane orientation. The formation of copper(II) acetate monolayers for **Si-Cu1** is not dense enough to produce interferences under our experimental conditions. The Kiessig fringes [48] for **Si-Cu2** and **Si-Cu3** samples slightly emerge, combining fact that these samples feature the thicker and the rougher layers.

Non-specular XRR curve (ω-scans) measurements were also performed at a fix position of $2\theta = 0.4°$ ($Q_X = 0.57\ nm^{-1}$). With non-specular XRR measurements one can determine the mosaic spread structure of a thin film, by relating peak width (FWHM) at a fixed Q_Z. The notion of mosaicity is used to describe the misorientation in epitaxial thin film. Fig. 4b shows the variation of the FWHM for each sample. The Si–H FWHM (0.022°, Fig. 4 b.1), correlates well with perfect crystalline system values. [49] Moreover, the bimetallic-copper grafted samples exhibit a mosaic spread to 0.032°, showing an increase in each grafting cycle. All measured samples exhibit low FWHM values, indicating a low misorientation in the parallel plane to Si(100) and such increase is consistent with the roughness data obtained by AFM.

3.5. Cyclic voltammetry

Understanding the electrical properties of a monolayer on the silicon surface is crucial for development of molecular-based devices toward potential applications (e.g., electrical memory, sensors and transistors). Fig. 5, shows the voltammetric curves for **Si-Cu1** (first scan) recorded at 0.010 V/s, which exhibits three well defined waves that correspond to two cathodic signals at −0.15 V and −0.52 V and the appearance of only one anodic signal at −0.15 V. These signals are not present in the H-terminated Si(100) surface nor in the **Si–N** sample (S2, Supplementary Data) used as reference materials. The presence of the aforementioned redox couple is a

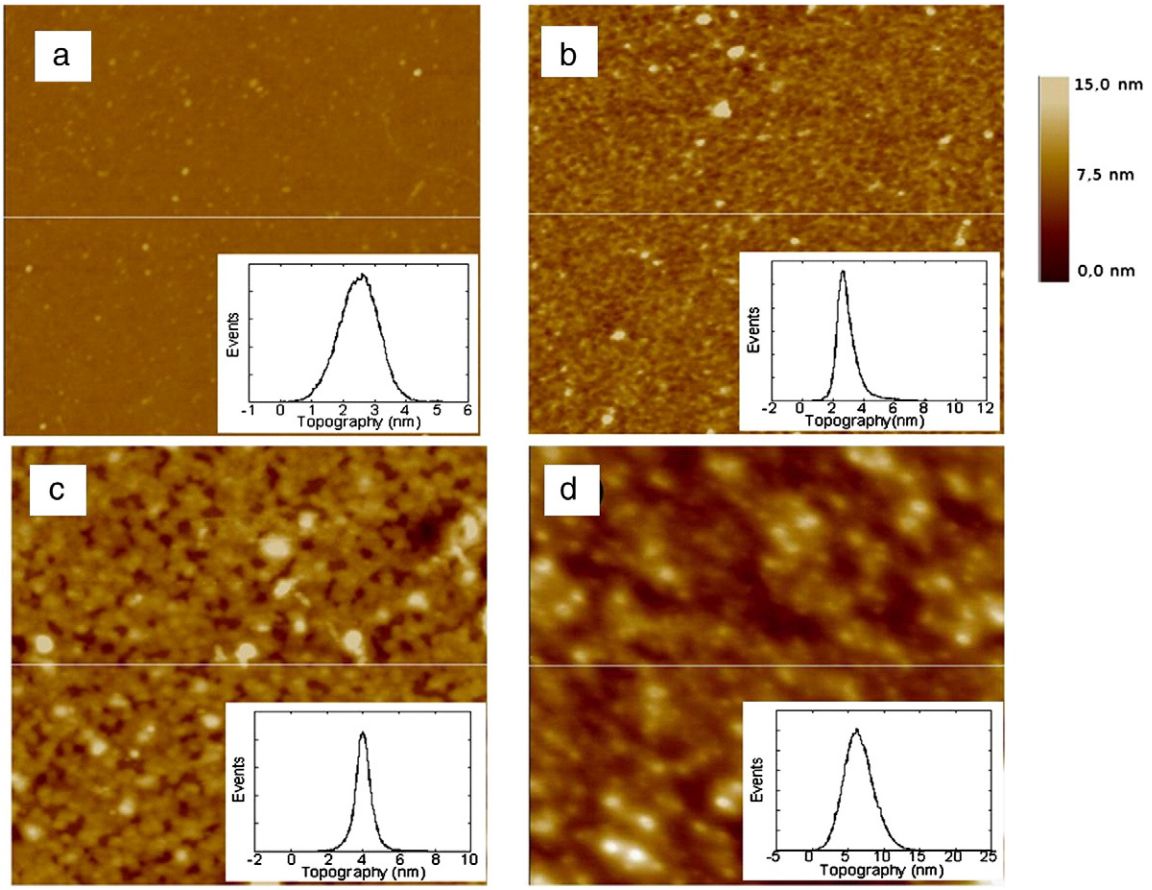

Fig. 3. AFM images of 1 μm × 1 μm of: a) **Si–N**, b) **Si-Cu1**, c) **Si-Cu2**, d) **Si-Cu3**. The insets correspond to the samples height profiles.

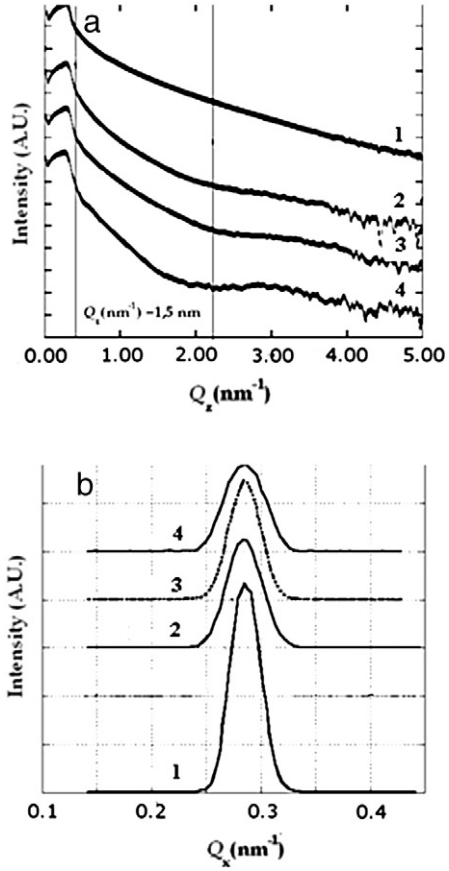

Fig. 4. a) XRR curve reflections and b) rocking curve profile analysis for: 1) **Si–H**, 2) **Si-Cu1**, 3) **Si-Cu2**, 4) **Si-Cu3** samples.

clear indication that copper(II) acetate molecules have been immobilized on the 4-aminopyridine on silicon surface, and are able to participate in the charge transfer process with the silicon electrode. It should be noted that blank experiments made using aniline instead of 4-aminopyridine grafted on silicon surface show no traces of the redox couple activity, thus indicating the key role of the N-terminal group to immobilize the complex.

After correcting the background charging current, the total charge withdrawn or injected to oxidize or reduce the monolayer can be determined from the area under the voltammetric wave. The second cathodic signal (−0.50 V) was not used for this calculation, because of the proximity with the amine desorption region (−0.95 V, S2, Support Information) produces a greater uncertainty in the calculation. The estimated charge from the integration of the anodic (−0.15 V) and cathodic signals (−0.15 V) of the first cycle, and slower scan rate (0.010 V/s) was taking as a measurement of the amount of electrochemically active copper(II) acetate complex immobilized in the SAMs. Interestingly, the oxidative estimated charge is approximately the double from the reductive charge (Table 1). This fact combined with complete irreversibility from the second cathodic signal, enables propose that Cu(II)/Cu(I) reduction occurred at −0.15 V, and Cu(I)/Cu(0) redox at −0.50 V, whereas the oxidation of Cu(0)/Cu(II) couple occurs in one stage at −0.15 V. Moreover, the difference between the two cathodic peaks for the individual one-electron reduction potentials, that is, Cu(II) to Cu(I) and Cu(I) to Cu(0) correspond to 0.35 V, and is very similar to the difference between copper standard reduction potential (0.37 V) [50], which supports this proposal. Furthermore, the shape of the voltammetric redox waves broadens, and could be originated due to two different Cu(II) ions present in copper(II) acetate.

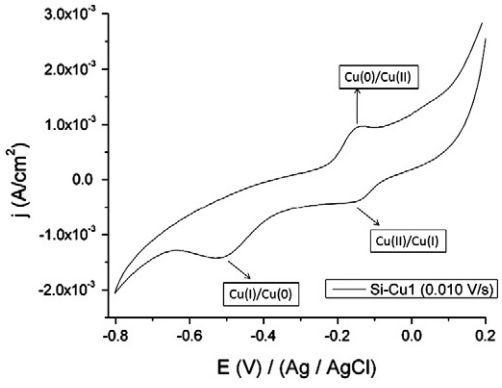

Fig. 5. Cyclic voltammogram of **Si-Cu1**, scan rate (0.010 V/s).

Surface-confined redox systems resemble the theoretically predicted ideal reversible behavior expected under DC cyclic voltammetry conditions and follows Nernstian type conduct. And, it is also assumed in such systems features as the symmetry between reduction and oxidation components (shape and magnitude) and coincidence peak-to-peak separation ($\Delta Ep = 0$). Furthermore, the peak currents are proportional to the potential scan rates. [51]

For the **Si-Cu1** samples, the behavior of the coupled signals at −0.15 V (cathodic signal) and −0.15 V (anodic signal) were electrochemically studied (Fig. 6).

As can be seen from Fig. 6a, ΔEp depends on the log scan rate. The zero separation between the position of the anodic peak (Ea) and the cathodic peak (Ec) at slower scans is consistent with a thermodynamically ideal surface system because of its electrochemical behavior, however, such separation increases significantly fast to 150 mV at 0.200 V/s, which corresponds to an almost irreversible system.

The rate of electron transfer in sample **Si-Cu1** can be defined as $k \approx \alpha n F \upsilon_c / RT = (1-\alpha) n F \upsilon_a / RT$, where υ_c and υ_a are slopes of plots of E_c and E_a versus log scan rate and α is a constant for a given system. Since $\Delta Ep > 200$ mV, the equation $\upsilon_a/\upsilon_c = \alpha/(1-\alpha)$ holds [51], and the values of υ_p obtained from the plot of Ep versus log of the scan rate yields $k \approx 2.9\ s^{-1}$, reflecting a slow electron transfer rate.

Significant alterations in the shape of the cyclic voltammetric curves are observed at higher scan rates and the plot peak current versus the scan rate is not linear.

The peak heights (Fig. 6b) were found to scale linearly with the scan rate rather than with $v^{1/2}$, ranging between 0.010 and 0.200 V/s, indicating a surface confined redox process where the scan rate and the current couple are described by Eq. (1):

$$i = \frac{n^2 F^2 A \Gamma v}{4RT}$$

In Eq. (1), n is the number of electrons transfer per ion (equivalents/mol), F is the Faraday's constant (C mol^{-1}); v is the scan rate (V/s), Γ corresponds to the number of redox sites (mol/cm^2, surface coverage), R is the gas constant (L atm mol^{-1} K^{-1}), and T is the temperature (K). [52] In this experiment, the reduction and oxidation current magnitudes observed with this technique are not identical. As previously mentioned, the estimated oxidative charge is approximately the double from the reductive charge at slower scan rates. It can also be calculated from the relationship

Table 1
Electrochemical relevant data for **Si-Cu1** sample. NC (not calculated).

Si-Cu1	First reduction wave	Second reduction wave	Oxidation
Charge (C/cm^2)	1.3×10^{-06}	NC	2.4×10^{-06}
Coverage (mol/cm^2)	1.4×1011	NC	1.3×10^{-11}
Peak position (V)	−0.15	−0.50	−0.15

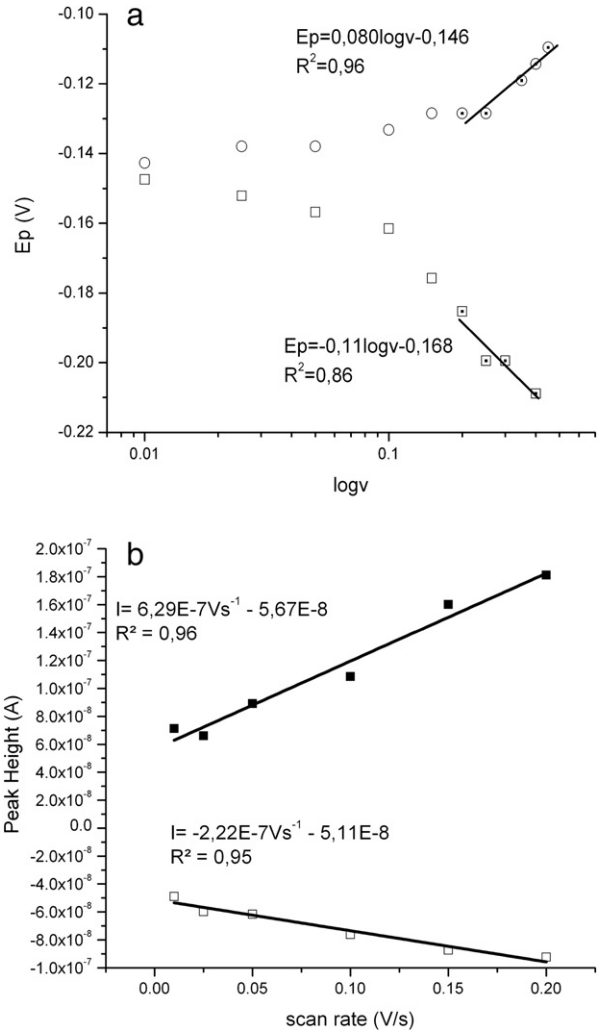

Fig. 6. Electrochemical experiments for Cu(II)/Cu(I) and Cu(II)/Cu(0) redox couples for **Si-Cu1** samples: a) peak current density as a function of CV log scan rates, b) peak heights a function of CV scan rates.

between the slope of anodic and cathodic peak height versus *v* a value of 2.83, a data that indicates the asymmetry between the anodic a cathodic electron transfer process. The coverage was calculating by Eq. (1) at low scan rate (0.010 V/s). Table 1 summarizes all electrochemical relevant data. The 1.4×10^{-11} mol/cm^2 of copper atom coverage (relationship between Cu and Si on the surface, 0.21 Cu: 13 Si) was calculated assuming an *n* equal 1 electrons and the reduction charge. Therefore, only a small fraction (approximately 10%) of the redox centers participates in the charge transfer process than the observed by XPS. At higher scan rates, the coverage changes toward even lower ones, this is hence consistent with the proposed slow kinetic phenomena and probably the charge transport rates are slower than the experimental time scale.

Si-Cu2 sample was also studied to gain a better insight of the electrochemical processes. As can be seen in Fig. 7, the voltammetric curves for sample **Si-Cu2** has three well defined and quantifiable waves at 0.500 V/s, as opposed to **Si-Cu1** voltammetric curves, which at the same scan rates are not possible to be observed due to high capacitances. These results could be related to low roughness for **Si-Cu1** as observed by AFM experiments; in contrast **Si-Cu2** roughness is higher and also shows lower capacitive conduct.

Table 2 summarizes all electrochemical relevant data for **Si-Cu2** (first scan) recorded at 0.010 V/s. The corresponding cathodic signal at −0.15 V and −0.51 V and the only one anodic signal at −0.14 V are very similar to the **Si-Cu1** sample. It can be assumed that the

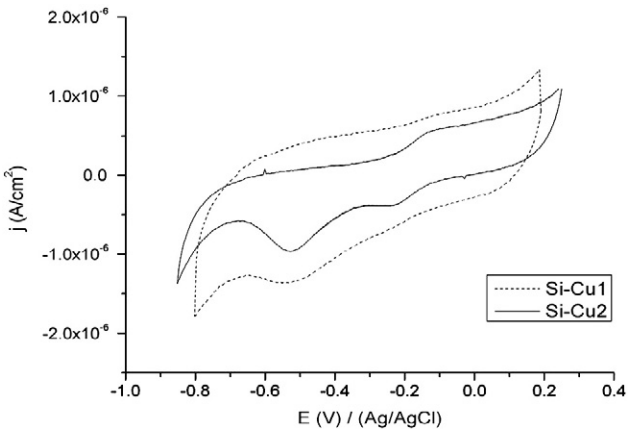

Fig. 7. Cyclic voltammograms of **Si-Cu1** and **Si-Cu2** samples (first scan) recorded at 0.500 V/s.

same redox processes are occurring and the Cu(II) chemical environment for **Si-Cu1** and **Si-Cu2** are almost the identical.

Fig. 8a, shows the ΔEp and current behavior as function of CV log scan rate for **Si-Cu2**. Remarkably, small Ep separation (10 mV) between the position of the anodic and cathodic peaks at slower scan is observed, and is consistent with a quasi-thermodynamically ideal surface for its electrochemical behavior. However, this separation increases with scan rate at 0.400 V/s to 90 mV, a fact which is characteristic of an almost reversible system. The plot of Ep versus log of the scan rate yield a $k\approx2.0\ s^{-1}$, reflecting even slower electron transfer rate than that for **Si-Cu1** sample.

The reversibility of **Si-Cu2** is generally higher when compared with **Si-Cu1**, and can be associated with the better sample measurement behavior, which in this context means smaller capacitance or absent of others non-faradic processes. It is worth mentioning that the stability of **Si-Cu2** bilayers was markedly more robust than the monolayer for **Si-Cu1**, presumably because of blockage of access to the surface of trace water that could initiate surface deterioration. [27]

The peak heights exhibit a linear dependence with the potential scan rate between 0.010 and 0.400 V/s, signalizing a surface confined redox process (Fig. 8b). The relationship between the slope of anodic and cathodic peak height versus *v* corresponds to 1.47, relating the asymmetry between the anodic a cathodic electron transfers, as observed also for **Si-Cu1** sample, however, in the case of **Si-Cu2** the relationship being nearly half of **Si-Cu1**. Thus, the estimated anodic coverage (1.2×10^{-11} mol/cm^2 of Cu(II) atoms) for the first cycle at slow scan rate (0.010 V/s) is slightly higher than the cathodic one (0.68×10^{-11} mol/cm^2 of Cu(II) atoms) (Table 2), assuming a 2 and 1 electron process, respectively. These facts show the increasing complexity of the electrochemical behavior of the bilayer (**Si-Cu2** sample), where process derivate from an inhomogeneity electroactive layer, or electronic coupling between adjacent molecules in the electroactive layer cannot be ruled out.

Finally, the experimental calculated coverage data are similar for **Si-Cu2** and **Si-Cu1** sample. At higher scan rates one notes coverage changes at even lower values. As previously pointed out, probably the limiting factor in the determination of the redox activity are very slow charge transport rates that are measured at a faster

Table 2
Electrochemical relevant data for **Si-Cu2** sample.

Si-Cu2	First reduction wave	Second reduction wave	Oxidation
Charge (C/cm^2)	6.6×10^{-07}	NC	2.3×10^{-06}
Coverage (mol/cm^2)	0.68×10^{-11}	NC	1.2×10^{-11}
Peak position (V)	−0.15	−0.51	−0.14

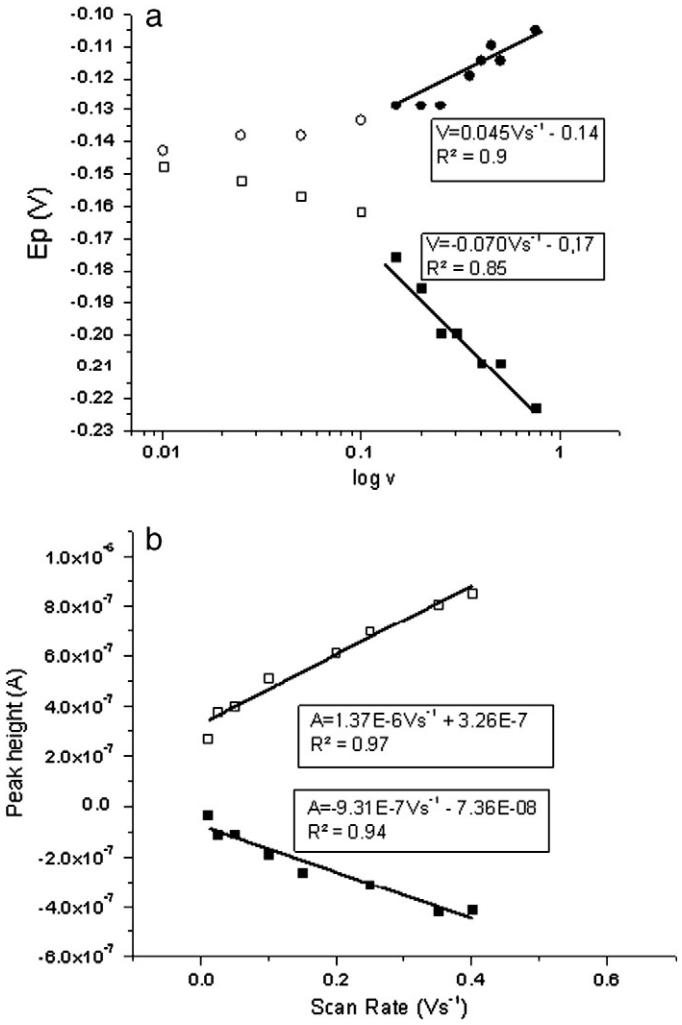

Fig. 8. a) Electrochemical experiments for Cu(II)/Cu(I) and Cu(II)/Cu(0) redox couples for **Si-Cu2** samples: a) peak current density as a function of CV log scan rates, b) peak heights a function of CV scan rates.

experimental time scale, and bringing about only a small fraction of the redox centers participate in the charge transfer process.

Si-Cu3 multilayers exhibit also electroactive features, that is, two cathodic signals at −0.13 V and −0.17 V, and one complete irreversible anodic wave at −0.55 V. One derives from these electrochemical data that it behaves in general similar to the **Si-Cu2** sample. (S3, Supplementary Data). The interconnection via the 4,4´ bipyridine appears to be able to participate in the charge transfer process with the silicon electrode.

4. Conclusion

In summary, we have successfully grafted copper acetate complex and demonstrated its versatility for controlled growing of monolayers and multilayers on silicon, through axial ligand exchange with amine linkers. One of the most promising features of hybrid devices is their use in nonvolatile memory technology, and potential advantages include unique capacitance (charge–voltage) and conductance (current–voltage) characteristics based on the multiple stable redox states that are accessible in an inorganic compound. The strategy of attaching copper redox multicenter opens the possibility of using these functionalized surfaces as storage medium; enabling the information being stored at discrete redox states of the molecules. We are currently studying these properties.

Finally, it can be anticipated that the controlled design of functional surfaces by applying the principles of bimetallic coordination chemistry not only opens new scientific perspectives but will also yield aesthetically appealing structures on surfaces. We have started out incorporating these findings to other multinuclear systems and further magnetic, electronic properties measurements and the use of microelectrodes will be published in due time.

Acknowledgments

This work was partially supported by CRUSA-CSIC grant, CONICIT-MICIT, and INTEL Costa Rica, especially thanks to Dr. Randolph Steinvorth for the constant support. The authors gratefully thank Mr. Sergio A. Paniagua from the Marder's research group at the Georgia Institute of Technology for the XPS analysis and useful discussions, Dr. Daniel Azofeifa (CICIMA), and Dr. Roberto Salvarezza from INIFTA, Argentina for their fruitful discussion. The help renders by Mr. Juan Diego Arias is greatly acknowledged.

References

[1] T. Strother, T. Knickerbocker, J.N. Russell, J.E. Butler, L.M. Smith, R.J. Hamers, Langmuir 18 (2002) 968.
[2] K.-C. Lin, I.-W.P. Chen, C. Chen, M.-H. Hsieh, C.-Y. Yeh, T. Lin, T.-H. Chen, S.-M. Peng, J. Phys. Chem. B 108 (1995) 959.
[3] F.A. Cotton, C. Lin, C.A. Murillo, Acc. Chem. Res. 9 (2001) 759.
[4] S. Rigaut, J. Perruchon, L. Le Pichon, D. Touchard, P.H. Dixneuf, J. Organomet. Chem. 670 (2003) 37.
[5] H. Fujihara, M. Ito, J. Mater. Chem. 15 (2005) 960.
[6] S. Leininger, B. Olenyuk, P. Stang, Chem. Rev. 10 (2000) 853.
[7] J. Berry, F.A. Cotton, L.M. Daniels, C.A. Murillo, J. Am. Chem. Soc. 124 (2002) 13212.
[8] R. Clérac, F.A. Cotton, L.M. Danniels, K.M. Dunbar, C.A. Murillo, I. Pascal, Inorg. Chem. 39 (2000) 752.
[9] F.A. Cotton, C.A. Murillo, X. Wang, Inorg. Chem. 38 (1999) 6294.
[10] A.A. Avey, R.H. Hill, J. Am. Chem. Soc. 118 (1996) 237.
[11] X. Cao, R.J. Hamers, J. Am. Chem. Soc. 123 (2001) 10988.
[12] X. Cao, S. Coulter, M. Ellison, H. Liu, J. Liu, J.R. Hamers, J. Phys. Chem. B 105 (2001) 3759.
[13] C. Mui, J.H. Han, G.T. Wang, C.B. Musgrave, S.F. Bent, J. Am. Chem. Soc. 124 (2002) 4027−4038.
[14] S.F. Bent, J. Phys. Chem. B 106 (2002) 2830.
[15] J. Buriak, J. Chem. Soc. Chem. Commun. (1999) 1051.
[16] S.P. Cummings, J. Savchenko, T. Ren, Coord. Chem. Rev. 255 (2011) 1587.
[17] G.M. Whitesides, R.F. Ismagilov, Science 284 (1999) 89.
[18] B.J. Eves, G.P. Lopinski, Surf. Sci. 579 (2005) L89.
[19] X.-Y. Zhu, V. Boiadjiev, J.A. Mulder, R.P. Hsung, R.C. Major, Langmuir 16 (2000) 6766.
[20] X.-Y. Zhu, J.A. Muder, W.F. Begerson, Langmuir 15 (1999) 8147.
[21] H.N. Waltenburg, J.T. Yates Jr., Chem. Rev. 95 (1995) 1589.
[22] N.Y. Kim, P.E. Laibinis, J. Am. Chem. Soc. 120 (1998) 4516.
[23] H. Habuka, T. Suzuki, S. Yamamoto, A. Nakamura, T. Takeuchi, M. Aihara, Thin Solid Films 489 (2005) 104.
[24] G. Shambat, A. Deberardinis, B. Chen, P. Reinke, B.J. Venton, L. Pu, J. Tour, J. Bean, Appl. Surf. Sci. 255 (2009) 8533.
[25] B. Fleury, L. Catala, V. Huc, C. David, W.Z. Zhong, P. Jegou, L. Baraton, S. Palacin, P.-A. Albouy, T. Mallah, Chem. Commun. (2005) 2020.
[26] H. Qi, A. Gupta, B.C. Noll, G.L. Snider, Y. Lu, C. Lent, T.P. Fehlner, J. Am. Chem. Soc. 127 (2005) 15218.
[27] K.M. Roth, A.A. Yasseri, Z. Liu, R.B. Dabke, V. Malinovskii, K.-H. Schweikart, L. Yu, H. Tiznado, F. Zaera, J.S. Lindsey, W.S. Kuhr, D.F. Bocian, J. Am. Chem. Soc. 125 (2003) 505.
[28] L. Wei, D. Syomin, R.S. Loewe, R.S. Lindsey, F. Zaera, D.F. Bocian, J. Phys. Chem. B 109 (2005) 6323.
[29] A.G. Marrani, E.A. Dalchiele, R. Zanoni, F. Decker, F. Cattaruzza, D. Bonifazi, M. Prato, Electrochim. Acta 53 (2008) 3903.
[30] S. Cordier, B. Fabre, Y. Molard, A.-B. Fadjie-Djomkam, N. Tournerie, A. Ledneva, N. G. Naumov, M. Moreac, P. Turban, S. Tricot, S. Ababou-Girard, C. Godet, J. Phys. Chem. C 114 (2010) 18622.
[31] B. Chen, M. Lu, A.K. Flatt, F. Maya, J.M. Tour, Chem. Mater. 20 (2008) 61.
[32] M. Yang, R.L.M. Teeuwen, M. Giesbers, J. Baggerman, A. Arafat, F.A. de Wolf, J.C.M. van Hest, H. Zuilhof, Langmuir 24 (2008) 7931.
[33] F. Cattaruzza, D. Fiorani, A. Flamini, P. Imperatori, G. Scavia, L. Suber, A.M. Testa, Chem. Mater. 17 (2005) 3311.
[34] J. Buriak, D. Wang, Langmuir 22 (2006) 6214.
[35] Y. Yamanoi, T. Yonezawa, N. Shirahata, H. Nishihara, Langmuir 20 (2004) 1054.
[36] K. Akamatsu, S. Ikeda, H. Nawafune, H. Yanagimoto, J. Am. Chem. Soc. 126 (2004) 10822.
[37] J. Kushmerick, Nature 462 (2009) 994.
[38] R.F. Service, Science 323 (2009) 1000.
[39] W.F. Begerson, J.A. Mulder, R.P. Hsung, X.-Y. Zhu, J. Am. Chem. Soc. 121 (1999) 454.

[40] D. Briggs, M. Seach (Eds.), Practical Surface Analysis by Auger and X-ray Photoelectron Spectroscopy, Wiley, New York, 1983.
[41] O. Cavalleri, G. Gonella, S. Terrini, M. Vignolo, L. Floreano, A. Morgante, M. Canepa, R. Rolandi, Phys. Chem. Chem. Phys. 6 (2004) 4042.
[42] E.J. Nemanick, P.T. Hurley, L.J. Webb, D.W. Knapp, D.J. Michalak, B.S. Brunschwig, J. Phys. Chem. B 110 (2006) 14470.
[43] R.L. Webb, M.L. Mino, E.L. Blinn, A. Pinkerton, Inorg. Chem. 32 (1993) 1396.
[44] D. Janssen, R. De Palma, S. Verlaak, P. Heremans, W. Dehaen, Thin Solid Films 515 (2006) 1433.
[45] I.M. Tidswell, B.M. Ocko, P.S. Pershan, S.R. Wassermann, G.M. Whitesides, J.D. Axe, Phys. Rev. B. 41 (1990) 1111.
[46] I.M. Tidswell, T.A. Rabedeau, P.S. Pershan, S.D. Kosowsky, J.P. Folkers, G.M. Whitesides, J. Chem. Phys. 95 (1991) 2854.
[47] T. Ishizaki, N. Saito, L. Sun-Hyung, K. Ishida, O. Takai, Langmuir 22 (2006) 9962.
[48] V. Holý, U. Pietsch, T. Baumbach, Springer-Verlag Editorial: Tracts in Modern Physics, 149, 1999, p. 119−127.
[49] M. Birkholz, Thin Film Analysis by X-Ray Scattering, Ed. WILEY-VCH Verlag GmbH: Weinheim. 2006.
[50] G.D. Christian, Analytical Chemistry, Wiley, New York, 2003.
[51] E. Laviron, J. Electroanal. Chem. 52 (1974) 355.
[52] D. Martel, N. Sojic, A. Kuhn, J. Chem. Educ. 79 (2002) 350.